

# Classification for the universal scaling of Néel temperature and staggered magnetization density of three-dimensional dimerized spin-1/2 antiferromagnets

D.-R. Tan,<sup>1</sup> C.-D. Li,<sup>1</sup> and F.-J. Jiang<sup>1,\*</sup>

<sup>1</sup>*Department of Physics, National Taiwan Normal University, 88, Sec.4, Ting-Chou Rd., Taipei 116, Taiwan*

Inspired by the recently theoretical development relevant to the experimental data of  $\text{TlCuCl}_3$ , particularly those associated with the universal scaling between the Néel temperature  $T_N$  and the staggered magnetization density  $M_s$ , we carry a detailed investigation of 3-dimensional (3D) dimerized quantum antiferromagnets using the first principles quantum Monte Carlo calculations. The motivation behind our study is to better understand the microscopic effects on these scaling relations of  $T_N$  and  $M_s$ , hence to shed some light on some of the observed inconsistency between the theoretical and the experimental results. Remarkably, for the considered 3D dimerized models, we find that the established universal scaling relations can indeed be categorized by the amount of stronger antiferromagnetic couplings connected to a lattice site. Convincing numerical evidence is provided to support this conjecture. The relevance of the outcomes presented here to the experiments of  $\text{TlCuCl}_3$  is briefly discussed as well.

PACS numbers:

## I. INTRODUCTION

While in general certain intriguing properties related to the phase transitions of classical models are governed by the thermal fluctuations, many interesting characteristics of different phases of quantum systems are trig-

gered by quantum fluctuations at zero temperature [1–5]. In other words, a great deal of attractive phenomena of quantum systems are observed at the low temperature regions where quantum fluctuations play the dominated roles in determining the properties of these systems. Still, for quantum systems, thermal fluctuations and the interplay between the effects from finite temperatures and zero temperatures may lead to compelling and fascinating results. A noticeable such an example is the quantum critical regime (QCR) associated with two-dimensional (2D) antiferromagnets [6–8].

Theoretically QCR is characterized by the appearance of several universal behavior among some physical quantities of the underlying 2D spin systems. In particular, this regime should be detectable at finite temperatures. Based on the relevant analytic calculations, for dimerized Heisenberg models, this regime should exist at any values of the tuning parameters associated with spatial anisotropy. Interestingly, while numerical studies of these models indicate the universal behavior associated with QCR can be observed with ease at the finite temperature regions above the related 2D quantum critical points (QCPs), such generic effects seem to disappear, or at least their existence are not firmly established yet, when the related calculations are carried out relatively away from QCPs [9–14]. To put it in another way, for quantum systems, the exotic characteristics of QCR can only be confirmed rigorously at the finite temperature regions above the associated QCPs where a dramatic change in the ground states occurs due to very strong quantum fluctuations. Although intuitively the thermal and ground state properties of a quantum system may seem to be unrelated to each other, close connections between these two categories of properties of that system may still exist.

Recently, the experimental results of  $\text{TlCuCl}_3$  have stimulated several theoretical investigation [15–25]. In particular, the phase diagram of  $\text{TlCuCl}_3$  under pressure motivates a few analytic and numerical explorations of three universal scalings between a thermal and a ground

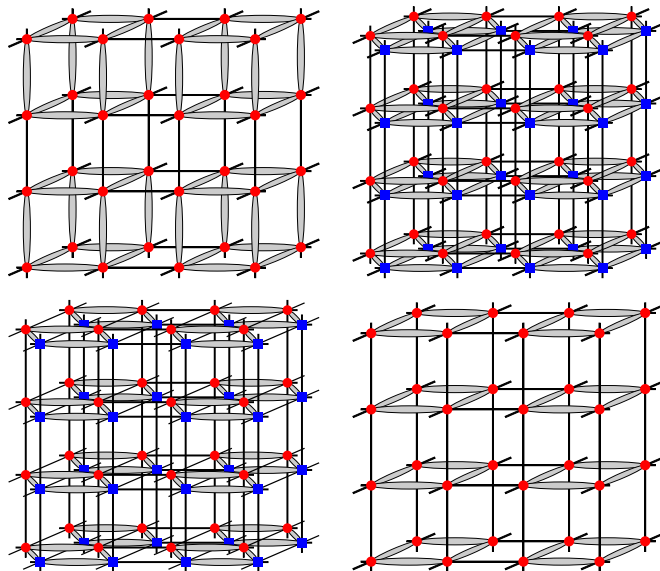


FIG. 1: The 3D dimerized spin-1/2 Heisenberg models investigated in this study: 3D cubical model (top left), double-cube-plaquette model (top right), double-cube-ladder model (bottom left), and 3D plaquette model (bottom right). Notice the antiferromagnetic coupling strength for the thick bonds and thin bonds are given by  $J'$  and  $J$ , respectively.

\*fjjiang@ntnu.edu.tw

state property of three-dimensional (3D) dimerized quantum antiferromagnets. Specifically, it is demonstrated that for three different 3D dimerized spin-1/2 Heisenberg models, the data collapse of the physical quantity  $T_N/T^*$  as functions of  $M_s$  leads to a universal curve [19]. In other words, for these three various dimerized systems, when the data of  $T_N/T^*$  are treated as functions of  $M_s$ , they fall on top of a smooth curve. Here  $T_N$  is the Néel temperature,  $T^*$  is the temperature where the observable uniform susceptibility  $\chi_u$  reaches its maximum value, and  $M_s$  is the staggered magnetization density. Similar smooth scaling appears as well if the quantity  $T_N/\bar{J}$  is considered instead of  $T_N/T^*$  [19]. Here  $\bar{J}$  is the summation of the antiferromagnetic coupling strength connected to a site of any of the studied dimerized models. Later it is shown that these scaling relations emerge as well for disordered systems [26, 27].

Although the agreement between the data of  $\text{TlCuCl}_3$  and the related analytic and numerical results is impressive, some controversial observations need to be clarified. For instance, while theoretically the appearance of smooth curves resulting from data collapse seems to support the scenario that generic scaling relations between  $T_N$  and  $M_s$  do exist, experimental data indicate these universal relations may depend on the microscopic details of the investigated models [15, 16, 21].

To uncover whether there indeed are generic scaling relations between  $T_N$  and  $M_s$  for 3D dimerized spin-1/2 antiferromagnets, in this study we conduct a large scale quantum Monte Carlo (QMC) calculation for several 3D spatially anisotropic spin-1/2 Heisenberg models. It is interesting to note the models studied in Ref. [19] that lead to universal data collapse have the following property. Specifically, among the antiferromagnetic bonds connected to a site, only one bond is of stronger coupling strength. Inspired by this observation, the considered 3D dimerized systems in this investigation can be classified by the amount of strong bonds touching a lattice site.

As anticipated, based on our numerical results, we find the established universal scaling relations mentioned above do appear for the models considered here. While the emergence of such scaling relations is foreseen, it is remarkable and unexpected that the data collapse using the related physical quantities of models having the same amount of strong bonds at each lattice site form their individual smooth universal curves. In particular, the universal scaling curves for models having different number of strong bonds per site differ from each other. In other words, the universal scaling considered in this study can be categorized by the amount of strong bonds connected to a lattice site.

The detailed investigation presented in this study not only reinforces the robustness of the known universal scaling between  $T_N$  and  $M_s$  for 3D dimerized quantum antiferromagnets, our results take these relations further by establishing quantitatively the classification of these relations. We would like to emphasize the fact that the outcomes shown here are useful for related experiments

as well. For example, by comparing the theoretical predictions and the associated data, one can propose the most applicable model for the targeted material. Moreover, this model can then be considered to explore some further theoretical properties of that material.

The rest of this paper is organized as follows. After the introduction, the studied 3D dimerized spin-1/2 models and the measured observables are briefly described. Then the obtained numerical data and the resulting analysis outcomes are summarized. In particular, the evidence to support the conjecture regarding the classification of the considered universal scaling relations outlined above is discussed in detail. Finally, a section is devoted to conclude the investigation presented here.

## II. MICROSCOPIC MODEL AND OBSERVABLES

The 3D dimerized quantum Heisenberg models investigated here are given by the Hamilton operators

$$H_1 = \sum_{\langle ij \rangle} J_{ij} \vec{S}_i \cdot \vec{S}_j + \sum_{\langle i'j' \rangle} J'_{i'j'} \vec{S}_{i'} \cdot \vec{S}_{j'}, \quad (1)$$

$$H_2 = \sum_i J_{\perp} \vec{S}_{i,1} \cdot \vec{S}_{i,2} + \sum_{\langle ij \rangle, \alpha=1,2} J_{ij,\alpha} \vec{S}_{i,\alpha} \cdot \vec{S}_{j,\alpha} \\ + \sum_{\langle i'j' \rangle, \alpha=1,2} J'_{i'j',\alpha} \vec{S}_{i',\alpha} \cdot \vec{S}_{j',\alpha}, \quad (2)$$

where in Eq. (1)  $J_{ij}$  and  $J'_{i'j'}$  are the antiferromagnetic couplings (bonds) connecting nearest neighbor spins  $\langle ij \rangle$  and  $\langle i'j' \rangle$  located at a 3D cubical lattice, respectively, and  $\vec{S}_i$  is the spin-1/2 operator at site  $i$ . Notice the  $\alpha$  in the second equation, which takes the value of either 1 or 2, stands for the indices of the considered two copies of 3D cubical lattices. In addition, the  $J_{\perp}$  appearing above are the couplings connecting spins that belong to different copies of the two targeted 3D cubical lattices. Finally, the other parameters and the operators showing up in Eq. (2) have the same definitions as their counterparts without the subscript  $\alpha$  in Eq. (1). It should be pointed out that in this study, we have set  $J_{ij} = J_{ij,1} = J_{ij,2} = J$  and  $J'_{i'j'} = J'_{i',j',1} = J'_{i',j',2} = J_{\perp} = J'$  with  $J' > J$  for any  $\langle ij \rangle$  and  $\langle i'j' \rangle$ . Figure 1 demonstrates the four dimerized spin-1/2 models studied here. Notice for the models of the top (bottom) two panels in fig. 1, among the bonds touching each lattice site, three (two) of them have larger magnitude in antiferromagnetic strength than the others. For convenience, in this investigation the models in fig. 1 will be called 3D cubical model (top left), double-cube-plaquette model (top right), double-cube-ladder model (bottom left), and 3D plaquette model (bottom right), respectively. Finally, since the couplings  $J'$  and  $J$  satisfy  $J' > J$ , each of the investigated system will undergo a quantum phase transition when the corresponding ratio  $J'/J$  exceeds a particular value.

To determine the Néel temperature  $T_N$ , the staggered magnetization density  $M_s$ , as well as  $T^*$  of the considered dimerized models, the observables staggered structure factor  $S(\pi, \pi, L_1, L_2, L_3)$  on a finite lattice with linear sizes  $L_1, L_2$ , and  $L_3$  are measured. In addition, both the spatial and temporal winding numbers squared ( $\langle W_i^2 \rangle$  for  $i \in \{1, 2, 3\}$  and  $\langle W_i^2 \rangle$ ), spin stiffness  $\rho_s$ , first Binder ratio  $Q_1$ , and second Binder ratio  $Q_2$  are calculated in our simulations as well. The quantity  $S(\pi, \pi, L_1, L_2, L_3)$  takes the form

$$S(\pi, \pi, L_1, L_2, L_3) = 3\langle (m_s^z)^2 \rangle, \quad (3)$$

where  $m_s^z = \frac{1}{L_1 L_2 L_3} \sum_i (-1)^{i_1+i_2+i_3} S_i^z$  with  $S_i^z$  being the third-component of the spin-1/2 operator  $\vec{S}_i$  at site  $i$ . Moreover, the spin stiffness  $\rho_s$  has the following expression

$$\rho_s = \frac{1}{3} \sum_{i=1,2,3} \rho_{si} = \frac{1}{3\beta} \sum_{i=1,2,3} \frac{\langle W_i^2 \rangle}{L_i}, \quad (4)$$

where  $\beta$  is the inverse temperature. Finally the observables  $Q_1$  and  $Q_2$  are defined by

$$Q_1 = \frac{\langle |m_s^z| \rangle^2}{\langle (m_s^z)^2 \rangle} \quad (5)$$

and

$$Q_2 = \frac{\langle (m_s^z)^2 \rangle^2}{\langle (m_s^z)^4 \rangle}, \quad (6)$$

respectively. With these observables, the physical quantities required for our study, namely  $T_N$ ,  $M_s$ , and  $T^*$ , can be calculated accurately.

### III. THE NUMERICAL RESULTS

To understand the robustness of the scaling relations associated with  $T_N$  and  $M_s$ , namely to uncover the rules of under what conditions the data collapse employing results from different models will lead to the same universal curves, we have carried out a large-scale QMC simulation using the stochastic series expansion (SSE) algorithm with very efficient loop-operator update [28]. Before presenting the numerical outcomes obtained from the QMC simulations, it should be pointed out that in our calculations related to the double-cube-plaquette model (double-cube-ladder model), due to the spatial arrangement of its antiferromagnetic bonds, the linear box sizes (size)  $L_1$  and  $L_2$  ( $L_1$ ) used in the simulations are twice that of  $L_3$  (those of  $L_2$  and  $L_3$ ) for most of the considered  $J'/J$  ( $J'/J \geq 4.6$ ) [29]. This strategy guarantees the aspect ratios among the three spatial winding numbers squared are kept within certain range. Consequently the 3D features of these models are preserved. For the 3D cubical model and the 3D plaquette model, the condition  $L_1 = L_2 = L_3$  is used in the related calculations.

In the following, we will firstly detail the determination of  $M_s$ .

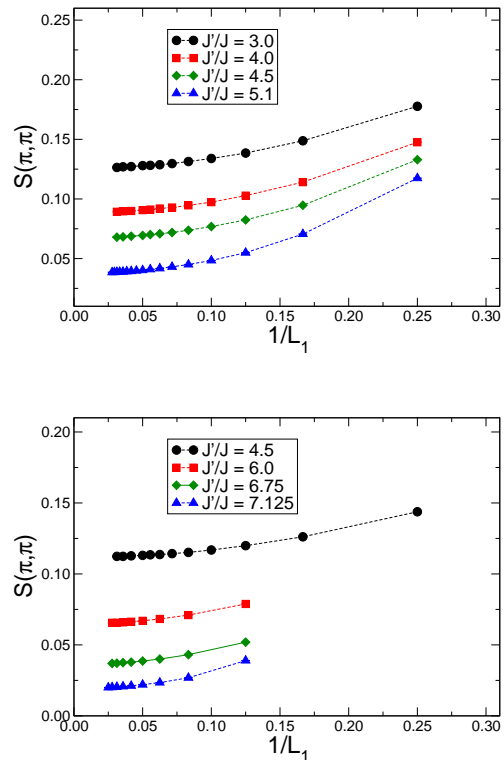


FIG. 2: The  $1/L_1$  dependence of the staggered structure factors  $S(\pi, \pi)$  for several considered  $J'/J$  of the 3D cubical model (top panel) and the double-cube-plaquette model (bottom panel). The dashed lines are added to guide the eye.

#### A. The determination of $M_s$

The observable considered for the calculations of  $M_s$  is  $S(\pi, \pi)(L_1)$  [30]. Specifically, for a given  $J'/J$ , the associated  $M_s$  is given by  $\sqrt{S(\pi, \pi)(L_1 \rightarrow \infty)}$ . We would like to point out that to determine  $M_s$  using this approach, the zero temperature, namely the ground state values of  $S(\pi, \pi)(L_1)$  are required. Therefore the simulations related to the calculations of  $M_s$  are conducted using the condition  $\beta = 2L_1$  [31]. For each of the considered models, we have additionally carried out several simulations (for some selected  $J'/J$ ) with  $\beta = 4L_1$ . The results obtained from these trial calculations agree very well with those determined by employing the relation  $\beta = 2L_1$  in the simulations.

For each of the studied model, the corresponding  $1/L_1$ -dependence of the ground state  $S(\pi, \pi)$  for some considered  $J'/J$  is depicted in figs. 2 and 3. Motivated by the theoretical predictions in Ref. [32], the determination of  $M_s$  is done by extrapolating the staggered structure factors at finite box sizes to their bulk results, using the following three ansatzes

$$a_0 + a_2/L^2, \quad (7)$$

$$b_0 + b_2/L^2 + b_3/L^3, \quad (8)$$

$$c_0 + c_2/L^2 + c_3/L^3 + c_4/L^4. \quad (9)$$

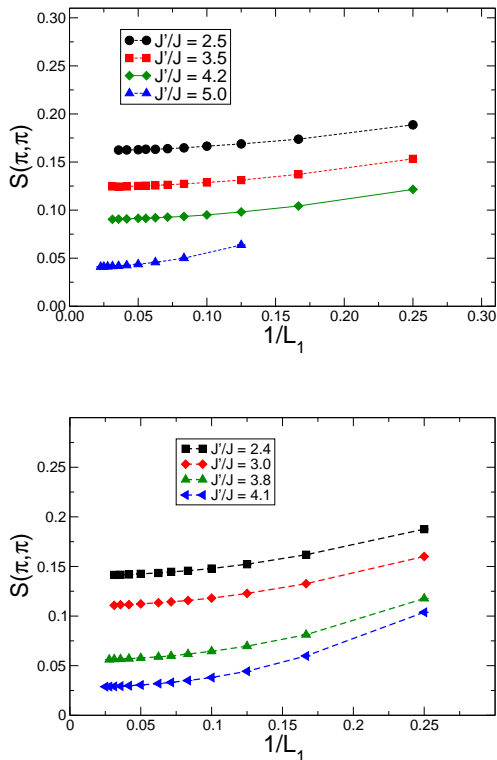


FIG. 3: The  $1/L_1$  dependence of the staggered structure factors  $S(\pi, \pi)$  for several considered  $J'/J$  of the double-cube-ladder model (top panel) and the 3D plaquette model (bottom panel). The dashed lines are added to guide the eye.

For each good fit ( $\chi^2/\text{DOF} \leq 2.0$ ), the corresponding bulk  $M_s$  is calculated by  $M_s = \sqrt{F}$  with  $F = a_0, b_0$ , or  $c_0$  depending on which ansatz is used for the fit. The numerical values of  $M_s$  determined from the fits employing ansatzes (7), (8), and (9) for all the four models are shown in figs. 4 and 5. The agreement between the results of  $M_s$  determined from different ansatzes is remarkably good, and the ones obtained with ansatz (8) are used in the following analysis.

We would like to emphasize the fact that since three spatial dimensions is the upper critical dimension of the quantum phase transitions investigated in this study, when approaching the critical points one expects to observe logarithmic corrections to  $M_s$  (and  $T_N$  as well). The theoretical calculations of the critical exponents associated with these logarithmic corrections are available in Refs. [22, 33, 34], and the predicted values are confirmed by careful analyses of  $M_s$  and  $T_N/\bar{J}$  conducted in Refs. [22, 27]. To perform an analysis associated with the mentioned logarithmic corrections requires data of  $M_s$  close to the related quantum critical points. Besides, the motivation of the investigation presented here is to understand to what extent the considered scaling relations are universal. Therefore, a detailed exploration of the logarithmic corrections related to the investigated phase transitions will be left for a future project.

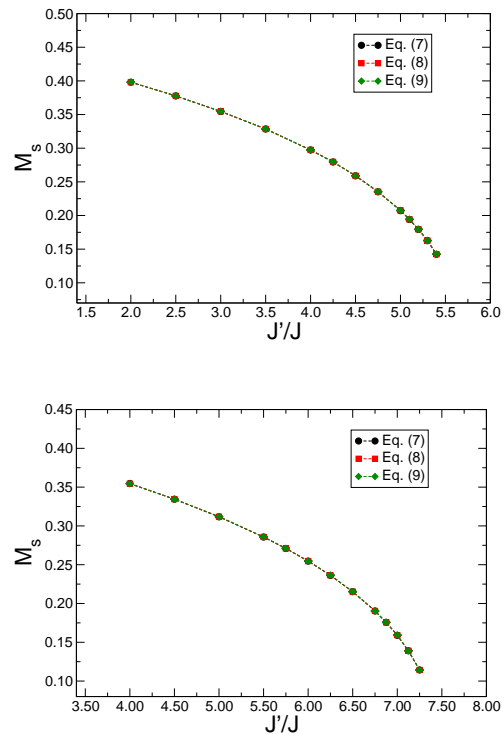


FIG. 4:  $M_s$  as functions of the considered  $J'/J$  for the 3D cubical model (top panel) and the double-cube-plaquette model (bottom panel). The dashed lines are added to guide the eye.

## B. The determination of $T_N$

The Néel temperatures  $T_N$  for various  $J'/J$  of the four studied models are calculated from the observables  $\rho_s L$  (which is given by  $(\sum_{i=1}^3 \rho_{si} L_i)/3$ ),  $Q_1$ , as well as  $Q_2$ . Notice bootstrap-type fits using constrained standard finite-size scaling ansatz of the form  $(1+b_0 L^{-\omega})(b_1 + b_2 t L^{1/\nu} + b_3 (t L^{1/\nu})^2 + \dots)$ , up to second, third, and (or) fourth order in  $t L^{1/\nu}$  are performed in the determination of  $T_N$ . Here  $b_i$  for  $i = 0, 1, 2, \dots$  are some constants and  $t = \frac{T - T_N}{T_N}$ . For some  $J'/J$ , ansatz up to fifth order in  $t L^{1/\nu}$  is used. The data of  $\rho_s L$ ,  $Q_1$ , and  $Q_2$  of some considered  $J'/J$  for the investigated models are shown in figs. 6 and 7.

In our analysis related to the calculations of  $T_N$ , a fit is treated as a good fit if the corresponding  $\chi^2/\text{DOF}$  satisfies  $\chi^2/\text{DOF} \leq 2.0$ . For few cases, in particular those associated with the observables  $\rho_s L$ , the criterion for good fits is slightly less restricted ( $\chi^2/\text{DOF} \leq 2.5$  is used for these situations). For every  $J'/J$  of each studied model, fits are carried out with ansatzes of various order in  $t L^{1/\nu}$ . Furthermore, for a given  $J'/J$ , several sets of data having different minimum box sizes are considered for the fits as well. The quoted values of  $T_N$  in this study are estimated by averaging the corresponding results of good fits. In addition, the error bar of each cited  $T_N$  is estimated conservatively from the uncertainty of every individual  $T_N$  of the associated good fits. The determined  $T_N$  from the

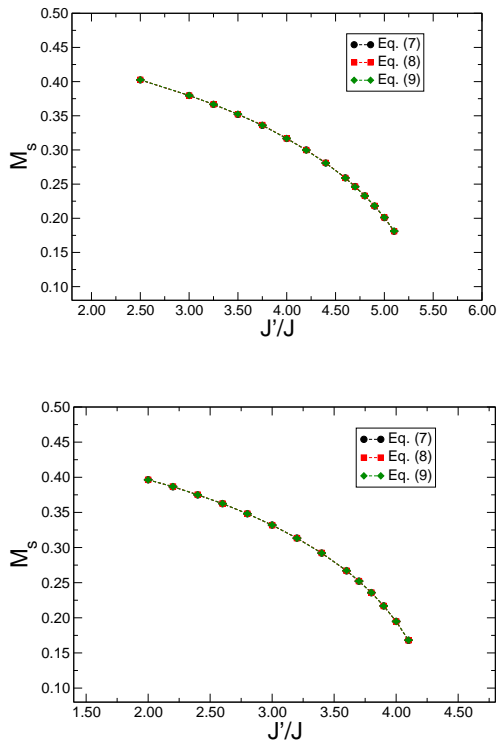


FIG. 5:  $M_s$  as functions of the considered  $J'/J$  for the double-cube-ladder model (top panel) and the 3D plaquette model (bottom panel). The dashed lines are added to guide the eye.

three used observables, namely  $\rho_s L$ ,  $Q_1$ , and  $Q_2$  for all the studied models are shown in figs. 8 and 9.

### C. The determination of $T^*$

For all the four investigated models, the corresponding  $T^*$ , namely the temperatures at which  $\chi_u$  reach their maximum value, are determined on lattices with moderate large box sizes such as  $(L_1, L_2, L_3) = (16, 16, 16)$ ,  $(24, 12, 12)$ , and so on. The obtained estimations of the inverse of  $T^*$  as functions of  $J'/J$  are shown in figs. 10 and 11. For each individual model, several additional simulations on lattice with larger or smaller box sizes than those associated with the results demonstrated in figs. 10 and 11 are conducted at some selected values of  $J'/J$ . These trial simulations confirm that for these selected  $J'/J$  the corresponding outcomes presented in figs. 10 and 11 are indeed the bulk results. Therefore the used  $T^*$  in the relevant analysis should be reliable.

### D. The scaling relations between $T_N/\bar{J}$ , $T_N/T^*$ , and $M_s$

Having obtained  $M_s$ ,  $T_N$ , and  $T^*$ , we now turn to study the scaling relation(s) between  $T_N/\bar{J}$  ( $T_N/T^*$ ) and

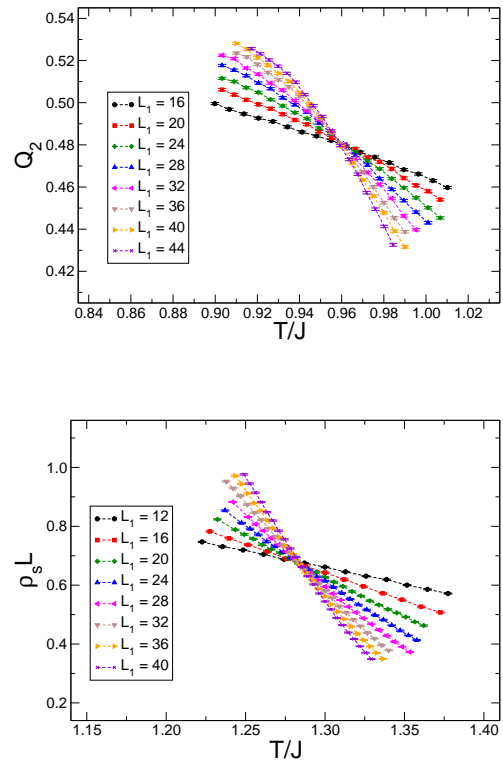


FIG. 6: Top panel:  $Q_2$  of the 3D cubical model as functions of  $T/J$  for  $J'/J = 5.0$  and  $L_1 = 16, 20, 24, 28, 32, 36, 40, 44$ . Bottom panel:  $\rho_s L$  of the double-cube-plaquette model as functions of  $T/J$  for  $J'/J = 6.5$  and  $L_1 = 12, 16, 20, 24, 28, 32, 36, 40$ .  $J$  is 1.0 in our calculations. The dashed lines are added to guide the eye.

$M_s$  ( $M_s$ ). Figure 12 shows  $T_N/J$  as functions of  $M_s$  for all the four considered models. The results in fig. 12 indicate there is no any universal relations for  $T_N/J$  and  $M_s$  among the investigated dimerized systems.

Remarkably, while no obvious scaling relations are observed when  $T_N/J$  are treated as functions of  $M_s$ , such universal dependence of  $T_N$  on  $M_s$  do emerge if the quantities  $T_N/\bar{J}$  and  $T_N/T^*$  are considered. This can be clearly seen in figs. 13 and 14. Specifically, the data of  $T_N/\bar{J}$  and  $T_N/T^*$  of these studied models do fall on top of their individual universal curves when these two quantities are regarded as functions of  $M_s$ . The most striking result shown in figs. 13 and 14 is that these universal scaling curves can be categorized by the amount of bonds which are connected to a lattice site and have the stronger antiferromagnetic coupling strength  $J'$ . Indeed, from the outcomes demonstrated in these figures, one can see that the universal curves corresponding to the 3D cubical model and the double-cube-plaquette model, which have three bonds of coupling strength  $J'$  at each of their lattice sites, are different from those of the 3D plaquette model and the double-cube-ladder model for which there are two bonds of coupling strength  $J'$  surrounding every

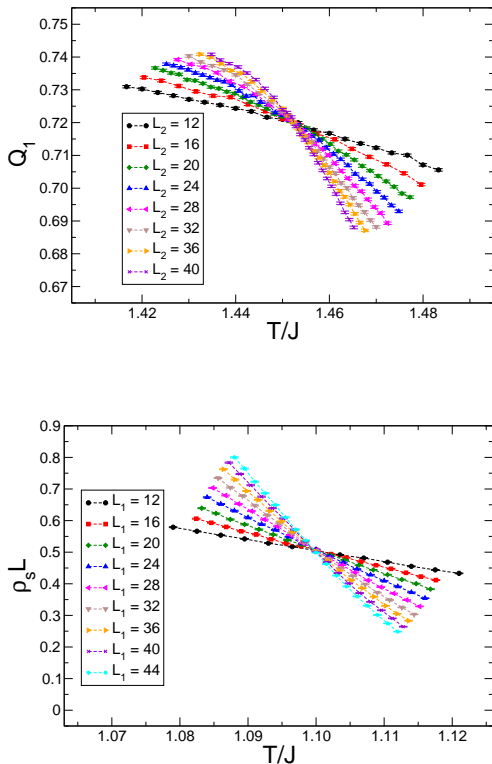


FIG. 7: Top panel:  $Q_1$  of the double-cube-ladder model as functions of  $T/J$  for  $J'/J = 3.5$  and  $L_2 = 12, 16, 20, 24, 28, 32, 36, 40$ . Bottom panel:  $\rho_s L$  of the 3D plaquette model as functions of  $T/J$  for  $J'/J = 3.0$  and  $L_1 = 12, 16, 20, 24, 28, 32, 36, 40, 44$ .  $J$  is 1.0 in our calculations. The dashed lines are added to guide the eye.

point of their underlying lattices. Notice for comparison purpose, the data of the 3D dimerized spin-1/2 ladder model [20], which has one strong bond per lattice site, are included in fig. 13 as well.

To conclude, figs. 13 and 14 show convincing evidence that the considered universal scaling relations investigated here can be categorized by the amount of stronger antiferromagnetic bonds touching any lattice site. We will argue later that this classification scheme regarding the studied universal scaling relations should be a generic one.

#### IV. DISCUSSIONS AND CONCLUSIONS

For certain types of 3D dimerized quantum antiferromagnets, it is demonstrated that universal scaling relations appear when the physical quantities  $T_N/\bar{J}$  and  $T_N/T^*$  are considered as functions of  $M_s$  [19]. Furthermore, near the associated quantum critical points, these mentioned observables scale linearly with  $M_s$ . Similar phenomena are observed for disordered models as well [26]. Motivated by these findings, in this study we have

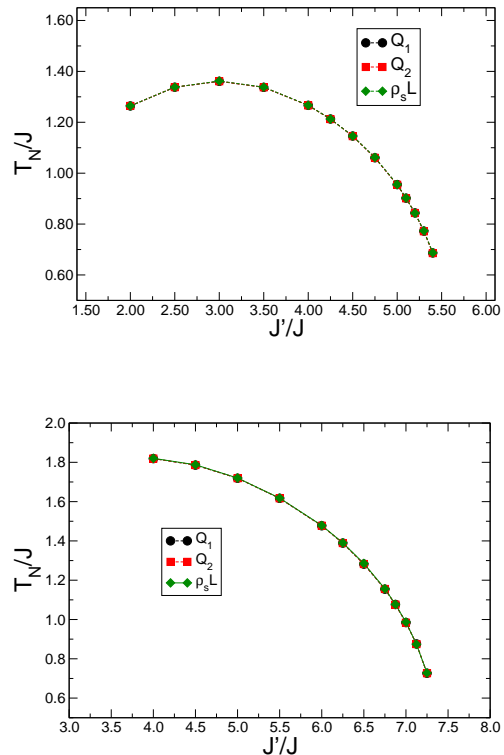


FIG. 8: The  $J'/J$  dependence of  $T_N$  obtained from  $Q_1$ ,  $Q_2$ , and  $\rho_s L$  for the 3D cubical model (top panel) and the double-cube-plaquette model (bottom panel), respectively.  $J$  is 1.0 in our simulations.

investigated four 3D dimerized spin-1/2 Heisenberg models, using the first principles nonperturbative quantum Monte Carlo simulations. Notice the models studied in Ref. [19] have the feature that among the bonds connected to every lattice site there is only one bond having stronger antiferromagnetic coupling strength. Based on this observation, for the models considered here, either two or three bonds surrounding a lattice site  $p$  possess stronger antiferromagnetic coupling strength than the others touching the same site  $p$ .

Remarkably, universal scaling relations associated with  $T_N$  and  $M_s$  do emerge for the four models studied here. In particular, among these four dimerized systems, the data collapse of  $T_N/\bar{J}$  and  $T_N/T^*$  of models having the same amount of strong bonds at each lattice site do form their individual smooth universal curves. Furthermore, the universal scaling curves of models having two strong bonds at each lattice site are different from those associated with models possessing three strong bonds per site. In other words, the universal scaling considered in this study can be categorized by the amount of strong bonds connected to a lattice site. Our findings considerably generalize those established in literature. It is interesting to notice the outcomes reached here are consistent with the experimental results of  $\text{TlCuCl}_3$ . Indeed the

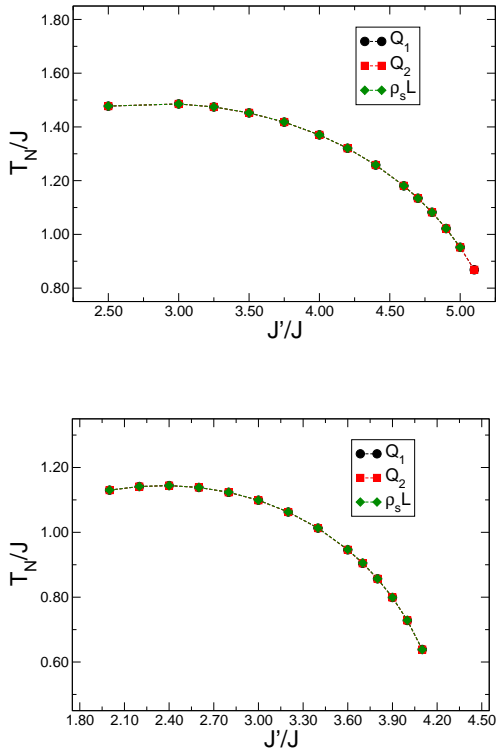


FIG. 9: The  $J'/J$  dependence of  $T_N$  obtained from  $Q_1$ ,  $Q_2$ , and  $\rho_s L$  for the double-cube-ladder model (top panel) and the 3D plaquette model (bottom panel).  $J$  is 1.0 in our simulations. Notice the  $T_N$  from  $\rho_s L$  for  $J'/J = 5.1$  of the double-cube-ladder model is not included in the sub-figure.

data of  $\text{TiCuCl}_3$  in Refs. [15, 16, 21] indicate the curves associated with the universal scaling of  $T_N/T^*$  and  $M_s$  most likely depend on the microscopic details of the studied systems. This is in agreement with the main result obtained in our investigation.

Finally we would like to point out that in Ref. [27], it is shown that for both a 3D spin-1/2 antiferromagnet with the so-called configurational disorder and the 3D regular dimerized ladder quantum Heisenberg model, data collapse of  $T_N/\bar{J}$  (as functions of  $M_s$ ) using the results from both systems leads to a smooth universal curve as well. Notice for a model with configurational disorder, each lattice site has exactly one strong bond for every disordered realization. Furthermore, while the number of bonds touching every site of the double-cube-type models

considered here is seven, the other two investigated models have six bonds connecting to any of their lattices. Based on these observations, it is likely that the results obtained here, namely the considered universal scaling relations of 3D dimerized spin-1/2 antiferromagnets can be categorized by the amount of strong bonds touching every lattice site, may be applicable for disordered systems and other lattice geometries. To verify whether this is indeed the case or not, simulating 3D antiferromagnets

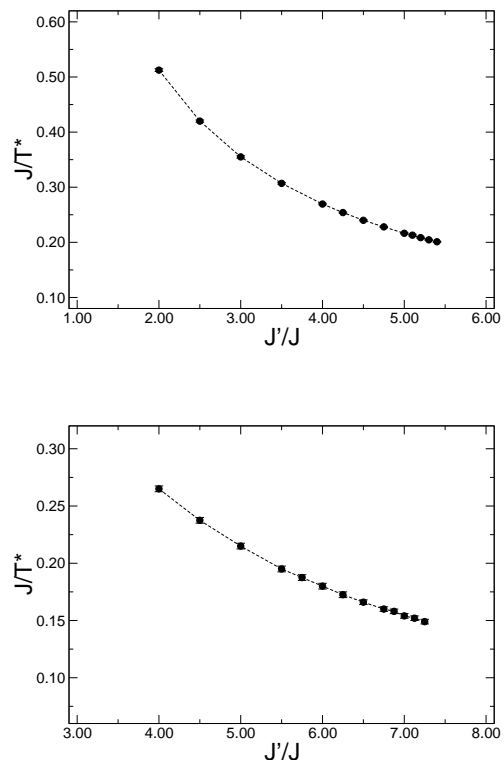


FIG. 10: The inverse of  $T^*$  as functions of  $J'/J$  for the 3D cubical model (top panel) and the double-cube-plaquette model (bottom panel).  $J$  is 1.0 in our simulations.

on the honeycomb lattice and other disordered models will shed some light on justifying this conjecture.

## V. ACKNOWLEDGMENTS

This study is partially supported by MOST of Taiwan.

- 
- [1] Nigel Goldenfeld, *Lectures On Phase Transitions And The Renormalization Group (Frontiers in Physics)* (Addison-Wesley, 1992).  
 [2] L. D. Landau and E. M. Lifshitz, *Statistical Physics Part 1, vol. 5 of Course of Theoretical Physics* (Pergamon Press, 3rd edition, 1994).

- [3] Lincoln D. Carr, *Understanding Quantum Phase Transitions (Condensed Matter Physics)* (CRC Press, 2010).  
 [4] S. Sachdev, *Quantum Phase Transitions* (Cambridge University Press, Cambridge, 2nd edition, 2011).  
 [5] Linda E. Reichl, *A Modern Course in Statistical Physics* (Wiley-VCH, 4th edition, 2016).

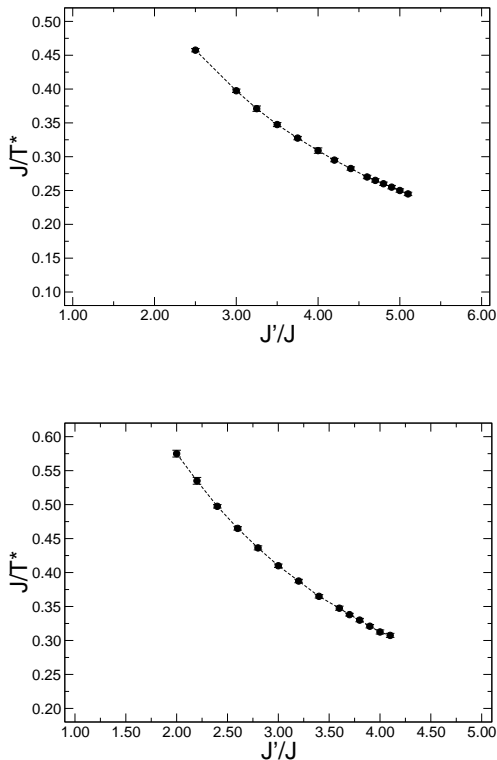


FIG. 11: The inverse of  $T^*$  as functions of  $J'/J$  for the double-cube-ladder model (top panel) and the 3D plaquette model (bottom panel).  $J$  is 1.0 in our simulations.

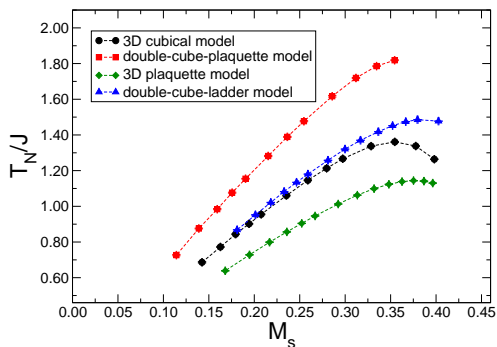


FIG. 12:  $T_N/J$  as functions of  $M_s$  for all the considered 3D dimerized models. The used values of  $T_N$  in the figure are from the observable  $Q_1$ .  $J$  is set to be 1.0 in our simulations.

- [6] A. V. Chubukov and S. Sachdev, Phys. Rev. Lett. **71**, 169 (1993).
- [7] A. V. Chubukov and S. Sachdev, Phys. Rev. Lett. **71**, 2680 (1993).
- [8] A. V. Chubukov, S. Sachdev, and J. Ye, Phys. Rev. B **49**, 11919 (1994).
- [9] A. W. Sandvik, A. V. Chubukov, and S. Sachdev, Phys. Rev. B **51**, 16483 (1995)

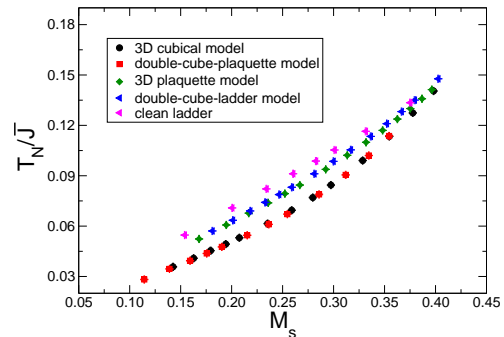


FIG. 13:  $T_N/\bar{J}$  as functions of  $M_s$  for all the considered models in this study. The used values of  $T_N$  in the figure are from the observable  $Q_1$ . For comparison purpose, some results of the 3D dimerized ladder model which has one strong bond per lattice site are included here as well [20].

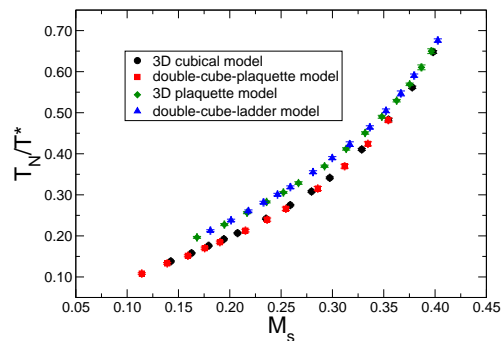


FIG. 14:  $T_N/T^*$  as functions of  $M_s$  for all the considered models in this study. The used values of  $T_N$  in the figure are from the observable  $Q_1$ .

- [10] M. Troyer, H. Kantani, and K. Ueda, Phys. Rev. Lett. **76**, 3822 (1996).
- [11] Matthias Troyer, Masatoshi Imada, and Kazuo Ueda, J. Phys. Soc. Jpn. **66**, 2957 (1997).
- [12] Jae-Kwon Kim and Matthias Troyer, Phys. Rev. Lett. **80**, 2705 (1998).
- [13] Y. J. Kim, R. J. Birgeneau, M. A. Kastner, Y. S. Lee, Y. Endoh, G. Shirane, and K. Yamada, Phys. Rev. B **60**, 3294 (1999).
- [14] Y. J. Kim and R. J. Birgeneau, Phys. Rev. B **62**, 6378 (2000).
- [15] Ch. Rüegg, N. Cavadini, A. Furrer, H.-U. Güdel, K. Krämer, H. Mutka, A. Wildes, K. Habicht, and P. Vorderwisch, Nature (London) **423**, 62, (2003).
- [16] Ch. Rüegg *et al.*, Phys. Rev. Lett. **100**, 205701 (2008).
- [17] Y. Kulik, and O. P. Sushkov, Phys. Rev. B **84**, 134418 (2011).
- [18] J. Oitmaa, Y. Kulik, and O. P. Sushkov, Phys. Rev. B **85**, 144431 (2012).
- [19] S. Jin and A. W. Sandvik, Phys. Rev. B **85**, 020409(R) (2012).

- [20] M.-T. Kao and F.-J. Jiang, Eur. Phys. J. B, (2013) 86: 419.
- [21] P. Merchant, B. Normand, K. W. Krämer, M. Boehm, D. F. McMorrow, and Ch. Rüegger, Nature physics **10**, 373-379 (2014).
- [22] Yan Qi Qin, Bruce Normand, Anders W. Sandvik, and Zi Yang Meng, Phys. Rev. B **92**, 214401 (2015).
- [23] Harley Scammell and Oleg Sushkov, Phys. Rev. B **92**, 220401 (2015).
- [24] Harley Scammell and Oleg Sushkov, Phys. Rev. B **95**, 024420 (2017).
- [25] Harley Scammell and Oleg Sushkov, Phys. Rev. B **95**, 094410 (2017).
- [26] Deng-Ruei Tan and Fu-Jiun Jiang, Eur. Phys. J. B, (2015) 88 : 289.
- [27] D.-R. Tan and F.-J. Jiang, Phys. Rev. B **95**, 054435 (2017).
- [28] A. W. Sandvik, Phys. Rev. B **66**, R14157 (1999).
- [29] For our calculations of  $M_s$  and  $T^*$  associated with the double-cube-plaquette model, all three spatial linear box sizes are equal for the simulations of  $J'/J = 4.0$  and  $4.5$ .
- [30] Since for a fixed  $J'/J$  of every considered model, the three linear box sizes  $L_1$ ,  $L_2$  and  $L_3$  are either equal or having fixed ratios, the abbreviations  $S(\pi, \pi)(L_1)$  and  $S(\pi, \pi)$  will be used for  $S(\pi, \pi, L_1, L_2, L_3)$  if no confusions may occur.
- [31] The values of  $\beta$  used for all the simulations with  $L \leq 10$  are  $\beta J = 24.0$ .
- [32] J. Cardy, *Scaling and Renormalization in Statistical Physics* (Cambridge University Press, Cambridge, 1996).
- [33] R. Kenna, Nucl. Phys. B **691**, 292 (2004).
- [34] R. Kenna, Vol. 3, Chap. 1, in *Order, Disorder and Criticality*, edited by Y. Holovatch, World Scientific, Singapore, 2012.